

Electronic Supplementary Information for

Silver nanoparticle aggregates on copper foil for reliable quantitative SERS analysis of PAHs with a portable Raman spectrometer

Xiaohong Jiang, Yongchao Lai, Min Yang, Heng Yang, Wei Jiang, Jinhua Zhan**
*Key Laboratory for Colloid & Interface Chemistry of Education Ministry, Department of
Chemistry, Shandong University, 250100 Jinan, China*

*Address for correspondence. Email: jhzhan@sdu.edu.cn

Phone: 86-531-88365017; Fax: 86-531-88366280

[Contents]

1. SEM image of silver nanoparticles on the copper foil for seven cycles.
2. SERS spectra of p-aminothiophenol on the substrate with different cycles.
3. Cross-sectional SEM image of the SERS substrate.
4. SEM image of dendritic silver on copper foil without the assistant of Sn²⁺.
5. SERS spectra of p-aminothiophenol on the SERS substrate with and without the assistant of Sn²⁺.
6. SERS and Raman spectra of HT.
7. The SERS spectra of HT with different immersion time.
8. Chemical structures of analytes in this work.
9. The calculated Raman spectra of PAHs.
10. The vibrational modes for main peaks of PAHs.
11. The temporal stability of the substrate under continuous laser radiation.

12. SERS spectra of fluoranthene obtained from the freshly prepared and aged substrate.

13. Qualitative SERS spectra of PAHs.

14. Detection limits, EF (Enhancement factor) and K_{OW} of PAHs.

15. Full Gaussian Reference.

1. SEM image of silver nanoparticles on the copper foil for seven cycles.

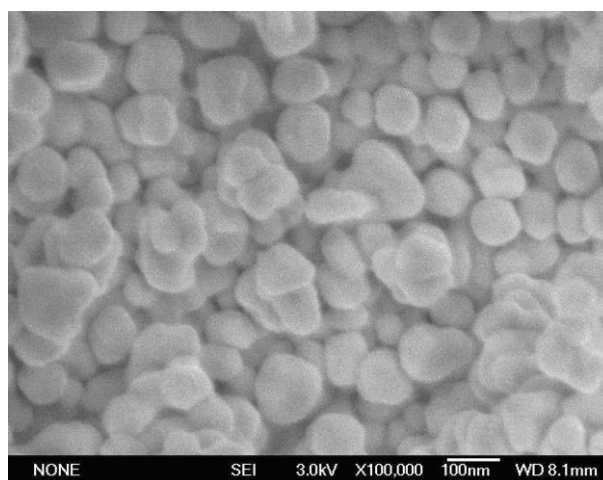


Fig. S1 SEM image of silver nanoparticles on the copper foil with the assistant of Sn^{2+} , for seven cycles.

2. SERS spectra of p-aminothiophenol on the substrate with different cycles.

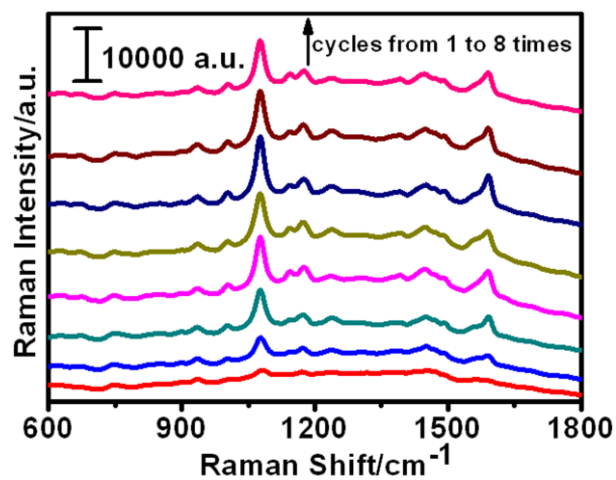


Fig. S2 SERS spectra of p-aminothiophenol (10^{-4} M) on the substrate with different cycles.

3. Cross-sectional SEM image of the SERS substrate.

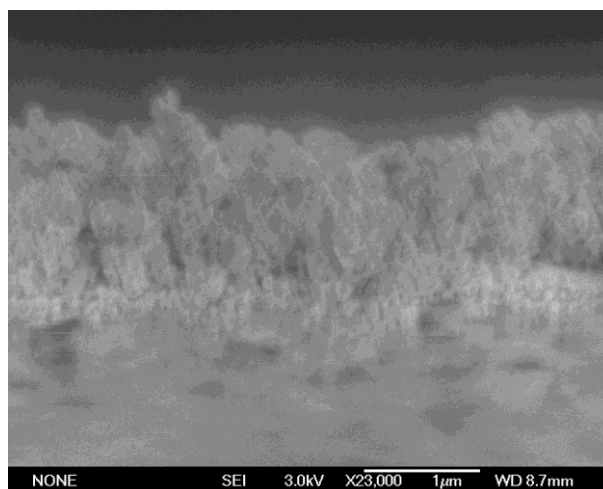


Fig. S3 Cross-sectional SEM image of the SERS substrate.

4. SEM image of dendritic silver on copper foil without the assistant of Sn^{2+} .

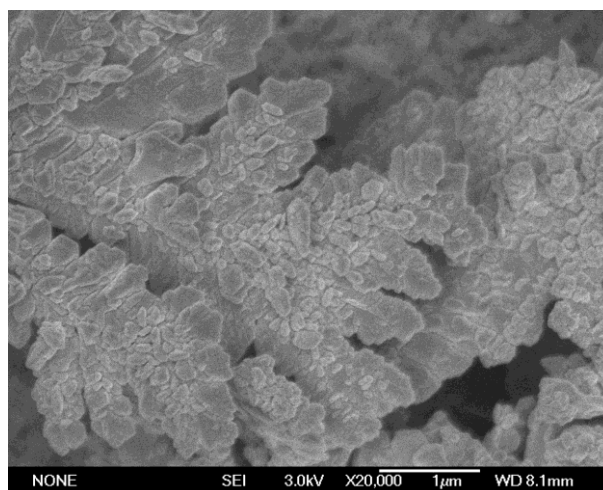


Fig. S4 SEM image of dendritic silver on copper foil without the assistant of Sn^{2+} .

5. SERS spectra of p-aminothiophenol on the SERS substrate with and without the assistant of Sn^{2+} .

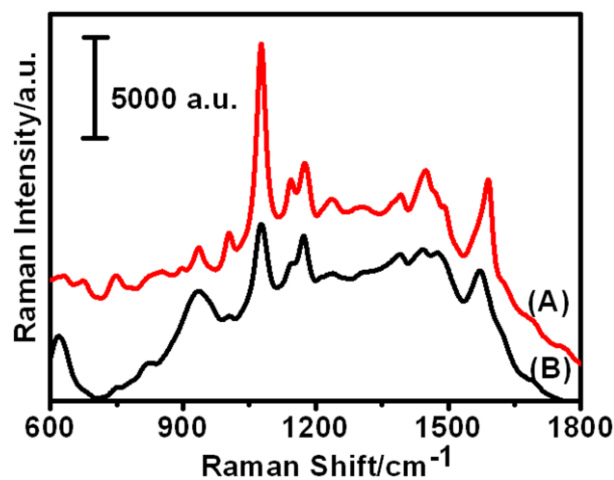


Fig. S5 SERS spectra of p-aminothiophenol (10^{-4} M) on the SERS substrate (A) with and (B) without the assistant of Sn^{2+} .

6. SERS and Raman spectra of HT.

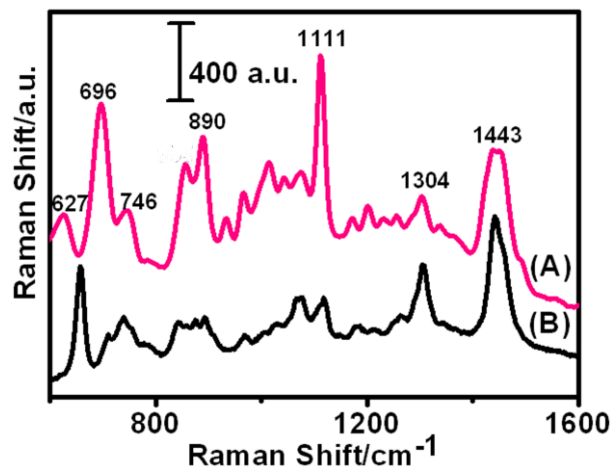


Fig. S6 (A) SERS spectrum of HT on the SERS substrate, (B) Raman spectrum of liquid HT served as a reference.

7. The SERS spectra of HT with different immersion time.

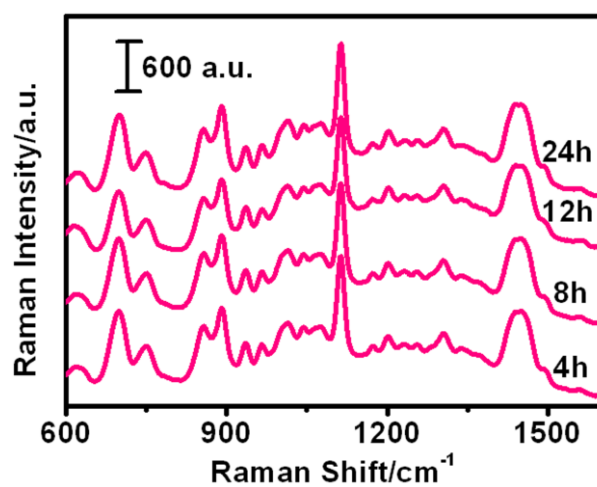


Fig. S7 The SERS spectra of HT with different immersion time.

8. Chemical structures of analytes in this work.

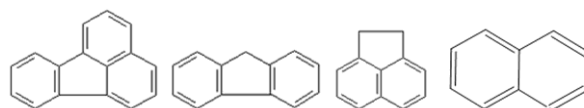


Fig. S8 Chemical structures of analytes in this work.

9. The calculated Raman spectra of PAHs.

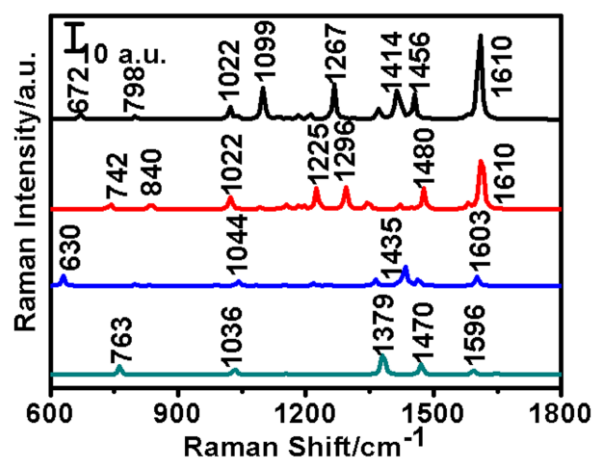


Fig. S9 The calculated Raman spectra of (A) fluoranthene, (B) fluorene, (C) acenaphthene, and (D) naphthalene.

10. The vibrational modes for main peaks of PAHs.

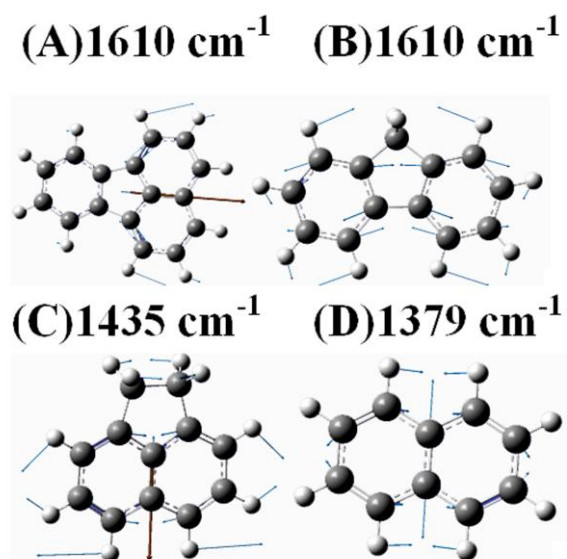


Fig. S10 The vibrational modes for main peaks of (A) fluoranthene at 1610 cm^{-1} , (B) fluorene at 1610 cm^{-1} , (C) acenaphthene at 1435 cm^{-1} , and (D) naphthalene at 1379 cm^{-1} .

11. The temporal stability of the substrate under continuous laser radiation.

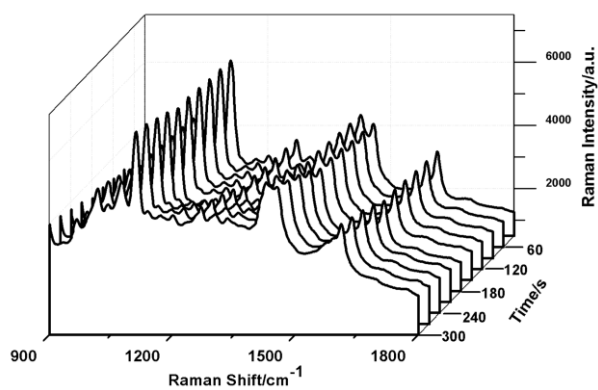


Fig. S11 The temporal stability of the substrate probed with $10^4\text{ }\mu\text{g}\cdot\text{L}^{-1}$ fluoranthene under continuous laser radiation for 5 min.

12. SERS spectra of fluoranthene obtained from the freshly prepared and aged substrate.

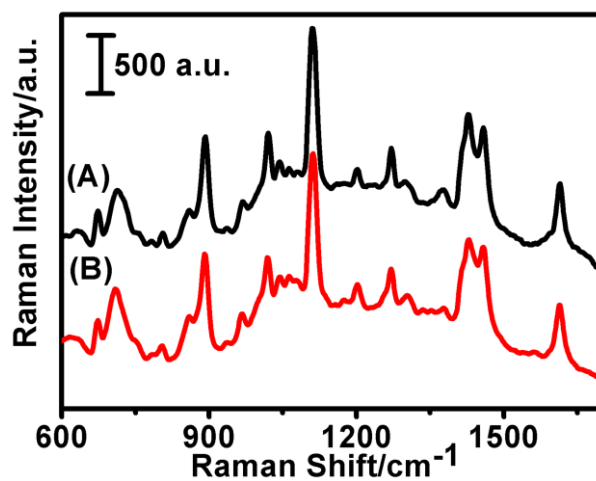


Fig. S12 SERS spectra of fluoranthene obtained from (A) the freshly prepared substrate and (B) the substrate immersed in the fluoranthene solution for 4 days.

13. Qualitative SERS spectra of PAHs.

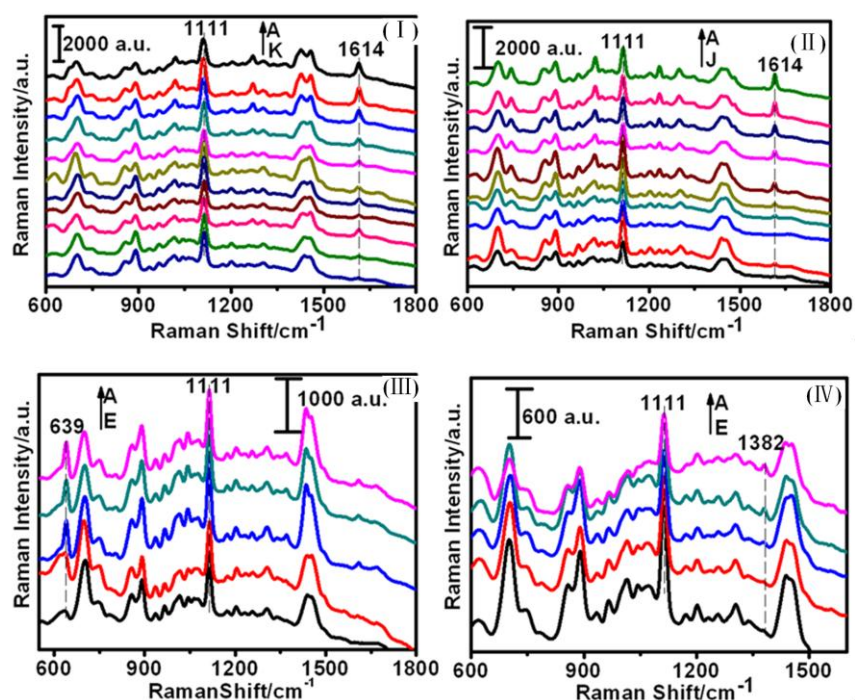


Fig. S13 SERS spectra for (I) fluoranthene with concentrations of (A) $1.0 \times 10^4 \mu\text{g}\cdot\text{L}^{-1}$, (B) $5.0 \times 10^3 \mu\text{g}\cdot\text{L}^{-1}$, (C) $2.5 \times 10^3 \mu\text{g}\cdot\text{L}^{-1}$, (D) $1.0 \times 10^3 \mu\text{g}\cdot\text{L}^{-1}$, (E) $5 \times 10^2 \mu\text{g}\cdot\text{L}^{-1}$, (F) $2.5 \times 10^2 \mu\text{g}\cdot\text{L}^{-1}$, (G) $10^2 \mu\text{g}\cdot\text{L}^{-1}$, (H) $50 \mu\text{g}\cdot\text{L}^{-1}$, (I) $25 \mu\text{g}\cdot\text{L}^{-1}$, (J) $10 \mu\text{g}\cdot\text{L}^{-1}$, and (K) $5.0 \mu\text{g}\cdot\text{L}^{-1}$, (II) fluorene with concentrations of (A) $1.0 \times 10^4 \mu\text{g}\cdot\text{L}^{-1}$, (B) $5.0 \times 10^3 \mu\text{g}\cdot\text{L}^{-1}$, (C) $2.5 \times 10^3 \mu\text{g}\cdot\text{L}^{-1}$, (D) $1.0 \times 10^3 \mu\text{g}\cdot\text{L}^{-1}$, (E) $5 \times 10^2 \mu\text{g}\cdot\text{L}^{-1}$, (F) $2.5 \times 10^2 \mu\text{g}\cdot\text{L}^{-1}$, (G) $10^2 \mu\text{g}\cdot\text{L}^{-1}$, (H) $50 \mu\text{g}\cdot\text{L}^{-1}$, (I) $25 \mu\text{g}\cdot\text{L}^{-1}$, (J) $10 \mu\text{g}\cdot\text{L}^{-1}$, (III) acenaphthene with concentrations of (A) $1.0 \times 10^4 \mu\text{g}\cdot\text{L}^{-1}$, (B) $5.0 \times 10^3 \mu\text{g}\cdot\text{L}^{-1}$, (C) $2.5 \times 10^3 \mu\text{g}\cdot\text{L}^{-1}$, (D) $1.0 \times 10^3 \mu\text{g}\cdot\text{L}^{-1}$, (E) $5 \times 10^2 \mu\text{g}\cdot\text{L}^{-1}$, (IV) naphthalene with concentrations of (A) $1.0 \times 10^4 \mu\text{g}\cdot\text{L}^{-1}$, (B) $5.0 \times 10^3 \mu\text{g}\cdot\text{L}^{-1}$, (C) $2.5 \times 10^3 \mu\text{g}\cdot\text{L}^{-1}$, (D) $1.0 \times 10^3 \mu\text{g}\cdot\text{L}^{-1}$, (E) $5 \times 10^2 \mu\text{g}\cdot\text{L}^{-1}$.

14. Detection limits, EF (Enhancement factor) and K_{OW} of PAHs.

Table S1 Detection limits, EF (Enhancement factor) and K_{OW} of PAHs.

PAHs	Detection limits ($\mu\text{g}\cdot\text{L}^{-1}$)	EF	log K_{OW}
fluoranthene	5.0	2.1×10^5	5.20
fluorene	10	3.7×10^4	4.23
acenaphthene	500	1.1×10^3	3.94
naphthalene	500	6.5×10^2	3.32

15. Full Gaussian Reference

M. J. Frisch, G. W. Trucks, H. B. Schlegel, G. E. Scuseria, M. A. Robb, J. R. Cheeseman, Jr. Montgomery, J.A.; T. Vreven, K. N. Kudin, J. C. Burant, J. M. Millam, S. S. Iyengar, J. Tomasi, V. Barone, B. Mennucci, M. Cossi, G. Scalmani, N. Rega, G. A. Petersson, H. Nakatsuji, M. Hada, M. Ehara, K. Toyota, R. Fukuda, J. Hasegawa, M. Ishida, T. Nakajima, Y. Honda, O. Kitao, H. Nakai, M. Klene, X. Li, J. E. Knox, H. P. Hratchian, J. B. Cross, V. Bakken, C. Adamo, J. Jaramillo, R. Gomperts, R. E. Stratmann, O. Yazyev, A. J. Austin, R. Cammi, C. Pomelli, J. W. Ochterski, P. Y. Ayala, K. Morokuma, G. A. Voth, P. Salvador, J. J. Dannenberg, V. G. Zakrzewski, S. Dapprich, A. D. Daniels, M. C. Strain, O. Farkas, D. K. Malick, A. D. Rabuck, K. Raghavachari, J. B. Foresman, J. V. Ortiz, Q. Cui, A. G. Baboul, S. Clifford, J. Cioslowski, B. B. Stefanov, G. Liu, A. Liashenko, P. Piskorz, I. Komaromi, R. L. Martin, D. J. Fox, T. Keith, M. A. Al-Laham, C. Y. Peng, A. Nanayakkara, M. Challacombe, P. M. W. Gill, B. Johnson, W. Chen, M. W. Wong, C. Gonzalez, and J.

A. Pople, Gaussian 03, Revision D.01; Gaussian, Inc., Wallingford CT, 2004.